Available online at www.sciencedirect.com
SCIENCE DIRECT®
ELSEVIER
Nuclear Instruments and Methods in Physics Research A ▮ (▮▮▮▮) ▮▮▮–▮▮▮
NUCLEAR INSTRUMENTS & METHODS IN PHYSICS RESEARCH Section A
www.elsevier.com/locate/nima

# Study of large area Hamamatsu avalanche photodiode in a γ-ray scintillation detector

T. Ikagawa[a,*], J. Kataoka[a], Y. Yatsu[a], T. Saito[a], Y. Kuramoto[a], N. Kawai[a], M. Kokubun[b], T. Kamae[c], Y. Ishikawa[d], N. Kawabata[d]

[a]*Tokyo Institute of Technology, 2-12-1 Ohokayama, Meguro, Tokyo 152-8551, Japan*
[b]*University of Tokyo, Tokyo, Japan*
[c]*Stanford Linear Accelerator Center, Menlo Park, CA, USA*
[d]*Hamamatsu Photonics K.K., Hamamatsu, Shizuoka, Japan*

Received 25 May 2004; received in revised form 24 August 2004; accepted 10 September 2004

**Abstract**

We have carried out study of a large area ($10 \times 10\,mm^2$), reverse-type avalanche photodiode (APD) recently developed by Hamamatsu photonics. It has low dark current of 3 nA at room temperature, and the gain stability was almost the same as prototypical APDs reported in our previous paper. We studied the performance as a γ-ray detector with four scintillators, CsI(Tl), BGO, GSO(Ce), and YAP(Ce) crystals. For example we obtained the best energy resolution of $4.9 \pm 0.2\%$ (FWHM) for 662 keV γ-rays, as measured with a $10 \times 10 \times 10\,mm^3$ CsI(Tl) crystal. The minimum detectable energy was as low as 10 keV at 20°C and 3.1 keV at −20°C. Thanks to its large effective area, this APD can effectively read out photons from larger size scintillators. When coupling to a $300 \times 48\,mm^2$ BGO plate of 3 mm thickness, an FWHM energy resolution of $20.9 \pm 0.2\%$ was obtained for 662 keV γ-rays, with the minimum detectable energy of about 60 keV at −15°C. These results suggest that our prototype APD can be a promising device for various applications replacing traditional PMTs such as use in space for Japan's future X-ray astronomy mission *NeXT*.


*PACS:* 07.85; 95.55.A; 85.60.D

*Keywords:* Avalanche photodiode; γ-rays; Scintillation detection

## 1. Introduction

In recent years, avalanche photodiodes (APDs) have attracted considerable attention as X-rays and γ-rays scintillation detectors in nuclear

*Corresponding author. Tel./Fax : +81 5734 2388.
*E-mail addresses:* ikagawa@hp.phys.titech.ac.jp (T. Ikagawa), kataoka@hp.phys.titech.ac.jp (J. Kataoka).

0168-9002/$ - see front matter © 2004 Elsevier B.V. All rights reserved.
doi:10.1016/j.nima.2004.09.021

physics. Compared with photomultiplier tubes (PMTs), APDs are compact, less sensitive to the magnetic field, and have rugged structures. Moreover, they have an excellent quantum efficiency (QE) ($\geqslant 80\%$) in the visible and near infrared. In previous works, three types of APDs, beveled edge, reach-through and reverse-type have been intensively studied [1,2], reverse-type APDs are the improved version of reach-through APDs [4]. They have a narrow, high-field multiple region close to the surface, which enables to obtain sufficient internal gain under relatively low bias voltage ($\sim$400 V [12]). In particular, reverse-type APDs have a good advantage of significantly, reducing dark noise, since the thermal electrons do not amplify inside the device. It has also been shown that reverse-type APDs are tolerant of nuclear radiation by CMS calorimeter in CERN [3,11].

In our previous paper, we have reported that Hamamatsu reverse-type APD, S8664-55, works at relatively low bias voltage of 300–350 V and have remarkably low dark current of $\sim$1 nA at room temperature. Their high QE and internal gain allow us to obtain good energy resolutions especially for the low-energy scintillation detection when coupled to CsI(Tl) crystals [5]. For example, the best FWHM resolutions of $9.4 \pm 0.3\%$ was obtained for 59.5 keV $\gamma$-rays from a $^{241}$Am source. 5.9 keV X-rays were clearly resolved at $-20^{\circ}$C with an energy resolution of $32.9 \pm 0.3\%$. In spite of many advantages, APDs have not been used widely because of their small effective area: commercial products of Hamamatsu APDs (S8664-55) have surface of $5 \times 5\,\mathrm{mm}^2$ at the maximum. To increase their effective area facilitates reading out X-rays and $\gamma$-rays with larger size scintillators and hence raises new possibilities for further applications.

Recently we have developed larger area, reverse-type APD ($10 \times 10\,\mathrm{mm}^2$) with Hamamatsu photonics. In this paper, we study the basic properties and performance as a $\gamma$-ray scintillation detector. In Section 2, we evaluate its basic parameters, such as gain stability and an excess noise factor. In Section 3 we examine the performance as a scintillation detector coupled with four small scintillators, CsI(Tl), BGO, GSO(Ce), and YAP(Ce) crystals. As an application, we use this APD to read out a large BGO plate scintillator ($300 \times 48\,\mathrm{mm}^2$; 3 mm thickness), which we plan to use for Japan's sixth X-ray astronomy mission *NeXT* (New X-ray Telescope) to effectively reject background $\gamma$-ray/particle events. Finally, we summarize our results in Section 4.

## 2. Properties of Hamamatsu APD: S8664-1010N

We have made two samples of large area ($10 \times 10\,\mathrm{mm}^2$) APD with Hamamatsu photonics (S8664-1010N). This APD is developed on the technical base of S8664-55 ($5 \times 5\,\mathrm{mm}^2$), except that the dead layer of S8664-1010N is thinner than that of S8664-55 [5]. These APDs have a narrow multiple region close to the front of the device, with a peak field only 7 μm deep. The Si wafer is placed on a ceramic board and the surface is coated with epoxy resin. The basic parameters of S8664-1010N are shown in Table 1. At a gain of 50, the leakage current is as low as 2.4/3.4 nA at 20°C and decreases to 52/60 pA at $-20^{\circ}$C. The detector capacitance is 266/268 pF, which is about three times larger than that of S8664-55 [5]. The QE is more than 80% between 500 and 830 nm and hence most sensitive at visible and near infrared. The QE decreases at ultraviolet due to absorption by the surface window.

### 2.1. Gain characteristics

As has been reported in the literatures, gain characteristics of APDs depend both on the bias

Table 1
Parameters of Hamamatsu APD (S8664-1010N: 2 pieces)

| | |
|---|---|
| Surface area | $10 \times 10\,\mathrm{mm}^2$ |
| Window | Epoxy resin |
| Dark current $I_D$[a] (at 20°C) | 3.4, 2.4 nA |
| Dark current $I_D$[a] (at $-20^{\circ}$C) | 52, 60 pA |
| Break-down voltage: $V_{brk}$ (at 25°C) | 426, 433 V |
| Bias: $V_{G=50}$[a] (at 20°C) | 376, 381 V |
| Capacitance: $C_{det}$[a] (at 20°C) | 268, 266 pF |
| Quantum efficiency | $\geqslant 80\%$ (500–830 nm)<br>60% (390 nm, 930 nm) |

[a]Measured at a gain of 50.

voltage and temperature [5]. We measured the APD gain by illuminating continuous light from a light emitting diode (LED) and recording the photocurrent of the APD as a function of bias voltage. At voltages lower than 50 V, the avalanche gain can be regarded as unity since the photocurrent remained constant.

Fig. 1 shows the gain variations of the APD as a function of bias voltage measured at several temperatures (from −20 to 20°C). We used a LED producing light signals of 525 nm. The gain increased with high voltage, reached to 2 at 200 V, 10 at 310 V, 50 at 381 V and 99 at 400 V at 20°C. When the APD device is cooled down, bias voltage required to achieve a certain gain is reduced because the probability of electron energy loss in interactions with phonons decreases. The electrons can obtain much more energy between each interaction and hence the avalanche gain increases [5]. The voltages where the gain reached to 50 were 381 V at 20°C and 350 V at −20°C.

As APD gain is expressed as an exponential function [6], the gain variations on bias voltage is approximated by

$$\frac{1}{M}\frac{\mathrm{d}M}{\mathrm{d}V} = 3.3\%/\mathrm{V} \tag{1}$$

at a gain of 50. Meanwhile the temperature dependence at the same gain is approximated by

$$\frac{1}{M}\frac{\mathrm{d}M}{\mathrm{d}T} = -2.5\%/^{\circ}\mathrm{C}. \tag{2}$$

These results are almost similar to those of S8664-55 and other traditional reverse-type APDs [3,5]. As is well known, temperature dependence of APDs is larger than those measured with typical PMTs (~0.3%). In order to stabilize gain at sufficiently small level compared to the energy resolutions of scintillators (Section 3), we controlled the temperature with an accuracy of less than 0.1°C in a thermostat. Corresponding variations of the gain is less than 0.3%.

Fig. 2 compares the gain variations measured at 20°C. We used LEDs with their peak emissions at 468, 525 and 637 nm for comparison. Gain reached to 50 at a bias voltage of 381 V for 468 and 525 nm LED, while 393 V for 637 nm LED. This suggests that electron hole (e–h) pairs created by shorter wavelength photons (468 and 525 nm) obtain full multiplication, whereas those of longer wavelength photons (637 nm) were not multiplied adequately.

Apparently, this is closely related with the internal structure of reverse-type APDs, where the thin high-field multiple region has been moved

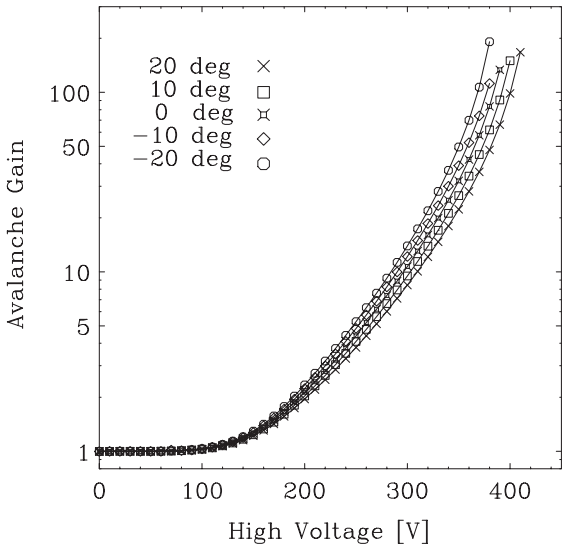


Fig. 1. Gain variations of S8664-1010N measured at various temperatures from −20 to 20°C.

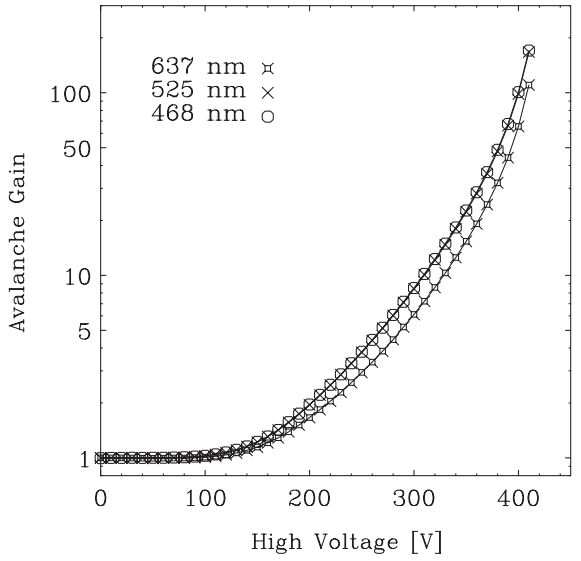


Fig. 2. Gain variations of S8664-1010N measured at various wavelength.

Table 2
Main properties of scintillators used for this experiment

| Crystal | Size ($mm^3$) | Decay time (ns) | Peak emission wavelength (nm) | Light yield (photons/keV) |
|---|---|---|---|---|
| CsI(Tl) | $10 \times 10 \times 10$ | 1005 | 550 | 61 |
| BGO | $10 \times 10 \times 10$ | 300 | 480 | 8–9 |
| GSO(Ce) | $10 \times 10 \times 10$ | 60 | 430 | 10 |
| YAP(Ce) | $10 \times 10 \times 10$ | 27 | 350 | 18.1 |

to the front end of the device surface. Longer wavelength photons penetrate through, or are absorbed in the avalanche region, obtaining relatively smaller gain compared to those for shorter wavelength photons. We note that the light emissions from the most popular scintillators peak at $\lambda \leqslant 550$ nm (e.g., CsI(Tl), GSO and BGO crystals; see Table 2), resulting in full multiplication.

### 2.2. Gains for LED and X-rays

Similarly X-rays could be absorbed further inside the avalanche region. Fig. 3 shows the energy spectrum featuring 5.9 keV X-rays, measured with S8664-1010N at 20°C. A 525 nm light pulser peak and the test pulser peak are also given in the same panel (see also Section 2.4).

The anode of the APD was connected to high-voltage supply (REPIC RPH 0022) through a 1 GΩ of resistance. Signals were read out from the anode of the APD, cutting DC component by a 2.2 nF of capacitor, collected by a charge-sensitive preamplifier CP581K provided by Clear Pulse Co., then passed a shaping amplifier ORTEC 570. After being converted to digital signals by an analog digital converter CP1114A provided by Clear Pulse Co., they were recorded on a computer.

We obtained the energy resolution of $10.4 \pm 0.2\%$ (FWHM) for 5.9 keV X-rays, which is better than the FWHM width of 14.1% recorded with S8664-55 [5]. Low-energy tail can clearly be seen in the spectrum, which corresponds to X-rays absorbed in the avalanche region. Fig. 4 compares the ratio of device gain for X-rays and LED light photons (525 nm). This result is very similar to those measured with S8664-55 [5], where the ratio is reduced with increasing the gain. The gain for

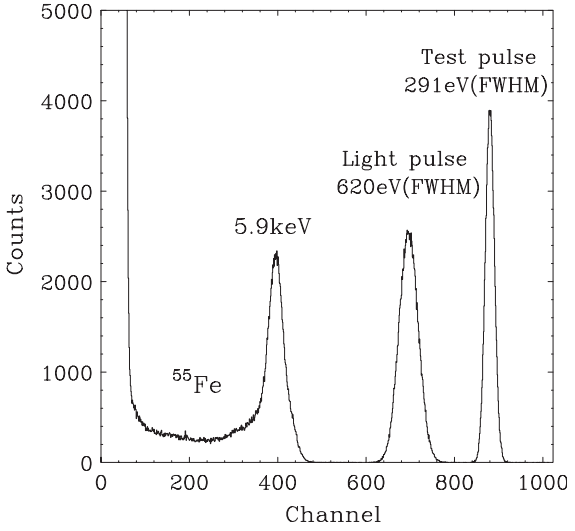


Fig. 3. The energy spectra of 5.9 keV X-rays, light pulse and test pulse measured with S8664-1010N.

X-rays is smaller by $32 \pm 5\%$ than those for LED ($\lambda = 525$ nm) at a gain of 50.

### 2.3. Gain uniformity

Uniformity of the device is important to achieve good performance, especially for large area APDs. We measured gain uniformity using a monochromatic X-ray beam at beamline BL-14A of the Photon Factory (KEK-PF) in Tsukuba, Japan. The APD was scanned with the collimated 6 keV X-ray beam ($1 \times 1\,mm^2$) at 2 mm intervals from 1 mm inner side of the edge to the other side. We obtained 25 points data in total. Operating bias voltage was 330 V and temperature was $24.1 \pm 0.1$°C. Fig. 5 shows a resulting "gain

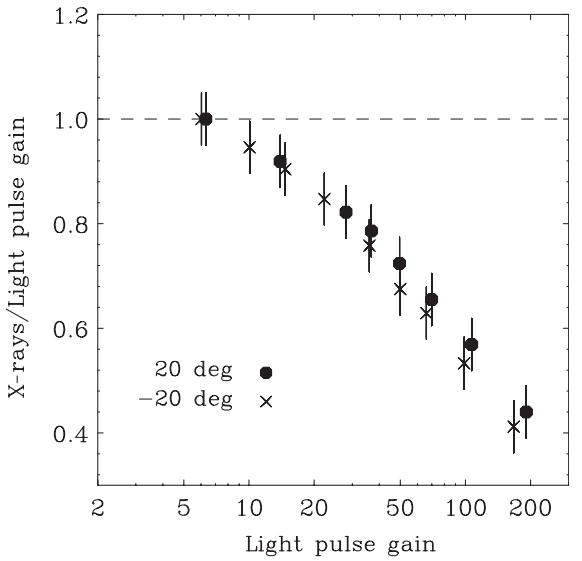


Fig. 4. The ratio of the APD gain for 5.9 keV X-rays and LED pulses measured for S8664-1010N.

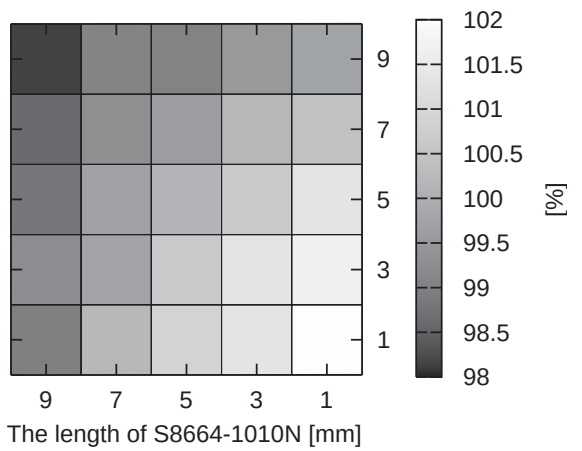


Fig. 5. The gain uniformity of S8664-1010N measured with a monochromatic 6 keV X-ray beam.

map'' shown in gray scale. The gain fluctuation was less than 2%, meaning that S8664-1010N has a good uniformity over whole surface area ($10 \times 10\,mm^2$). Such a small gain variation might be caused by non-uniformity of the wafer thickness and/or distortion of the electric field inside the device; further study is necessary to confirm this.

### 2.4. Excess noise factor

As shown in Fig. 3, the spectral width of light pulse measured with the APD is mainly determined by the statistical fluctuation related to avalanche multiplication, statistics of primary e–h pairs, and dark noise contribution. For the LED pulse illumination, the energy resolution $\Delta E$ of the LED light pulser peak is expressed by [2],

$$\Delta E^2 = (2.355)^2 FE\varepsilon + \Delta^2_{\mathrm{noise}} \quad (3)$$

where $E$ is the energy of the light peak in keV and $\Delta_{\mathrm{noise}}$ is the dark noise contribution of the measurement system. $\varepsilon$ is the energy per e–h pair creation (3.65 eV for Si). $F$ is an excess noise factor, which is a parameter describing avalanche fluctuation of the APD. In this calculation it is necessary to consider gain difference between 5.9 keV X-rays and LED photons (see Section 2.1). Combining Figs. 3 and 4, the corrected energy of the light pulse was 7.0 keV and the FWHM of the light pulse and test pulse were 620 and 291 eV, respectively. We, therefore, obtained an excess noise factor of $F = 1.5 \pm 0.1$, measured with 525 nm light pulse at a gain of 50. This excess noise factor is better than that of S8664-55 measured in our previous paper [5].

## 3. Performance as a scintillation photon detector

### 3.1. List of scintillators

In the scintillation detection, we study the performance of S8664-1010N with four different scintillators; CsI(Tl), BGO, GSO(Ce) and YAP(Ce) crystals. The size of the crystals was $10 \times 10 \times 10\,mm^3$ and can fully match the sensitive area of the APD. The crystals were wrapped with several layers of Teflon tape and were coupled with Si rubber sheet (100 μm thickness) directly to the entrance window of S8664-1010N. The main properties of the scintillators provided by manufacturers are listed in Table 2.

### 3.2. Performance at room temperature

First we study the performance of scintillation detector at 20°C. We also measured the pulse height spectra with the PMT for comparison (Hamamatsu R7899EG; 1 inch diameter), using the same scintillation crystals. Fig. 6 compares the pulse height spectra for 662 keV γ-rays from a $^{137}$Cs source, measured with the APD (*top*) and PMT (*bottom*), coupled to the same CsI(Tl) crystal. Thanks to a high QE, an excellent FWHM energy resolution of $4.9 \pm 0.2\%$ was obtained for the APD, whereas the PMT system shows a moderate energy resolution of $5.9 \pm 0.1\%$. Note that the energy resolution achieved with S8664-1010N is better or comparable with that obtained with S8664-55 ($5.2 \pm 0.3\%$).

More strikingly, APDs' internal gain reduces noise contribution of the electronic system significantly [5,10]. As can been seen in Fig. 6 both the APD and the PMT could resolve 32 keV X-ray peak. Note that PIN-photodiode plus CsI(Tl) system cannot resolve such low-energy X-rays due to the noise contribution. The energy resolutions for 32 keV X-rays was $20.6 \pm 0.2\%$ for the APD, which is comparable to the PMT case ($23.0 \pm 0.1\%$).

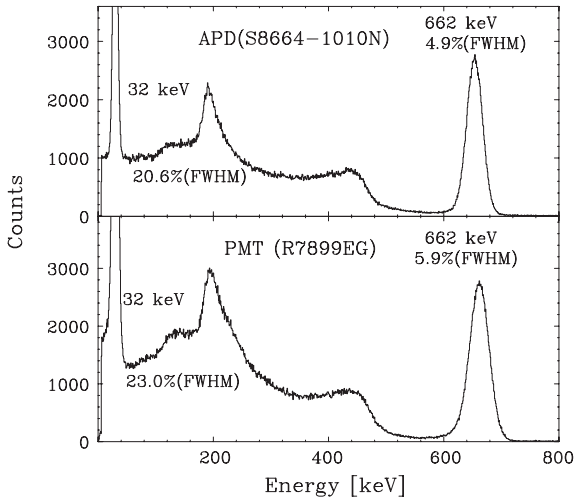


Fig. 6. (top) The energy spectrum of $^{137}$Cs measured with S8664-1010N coupled to a CsI(Tl) crystal. (bottom) The energy spectrum of $^{137}$Cs measured with R7899EG coupled to the same CsI(Tl) crystal. Both were measured at 20°C.

Figs. 7, 8 and 9 show the energy spectra of 662 keV γ-rays from a $^{137}$Cs source measured with the APD, coupled to BGO, GSO(Ce) and YAP(Ce) crystal, respectively. The FWHM energy resolutions for 662 keV γ-rays were $8.3 \pm 0.2\%$ for BGO, $7.8 \pm 0.2\%$ for GSO(Ce) and $11.3 \pm 0.3\%$

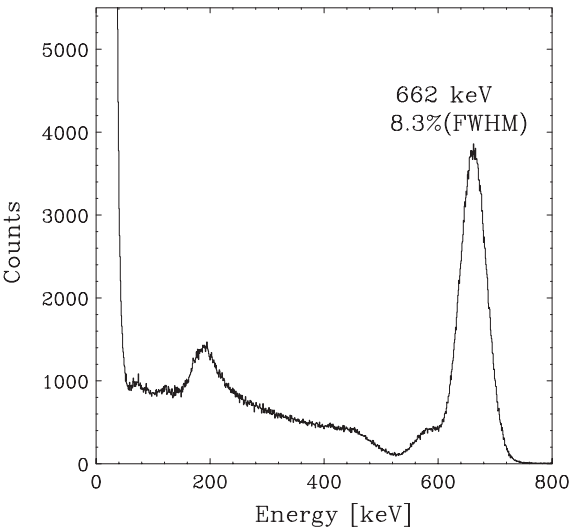


Fig. 7. The energy spectrum of $^{137}$Cs measured with S8664-1010N coupled to a BGO crystal measured at 20°C.

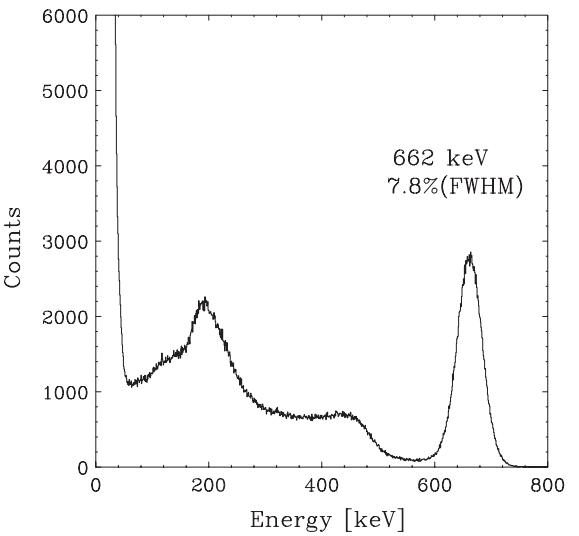


Fig. 8. The energy spectrum of $^{137}$Cs measured with S8664-1010N coupled to a GSO(Ce) crystal measured at 20°C.

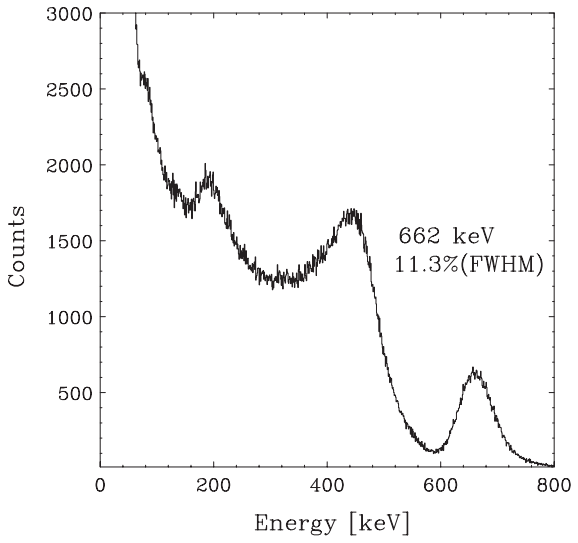


Fig. 9. The energy spectrum of $^{137}$Cs measured with S8664-1010N coupled to a YAP(Ce) crystal measured at 20°C.

Table 3
Comparison of energy resolutions measured with APD(S8664-1010N) and PMT (R7899EG) at 20°C

| Crystal | Shaping time | Energy resolution of 662 keV (%) | |
|---|---|---|---|
| | (μs) | APD | PMT |
| CsI(Tl) | 10 | 4.9 ± 0.2 | 6.0 ± 0.1 |
| BGO | 3 | 8.3 ± 0.2 | 10.4 ± 0.1 |
| GSO(Ce) | 1 | 7.8 ± 0.2 | 9.3 ± 0.1 |
| YAP(Ce) | 0.5 | 11.3 ± 0.3 | 12.4 ± 0.1 |

for YAP(Ce) crystals. These results were better than those obtained with the PMT; 10.4 ± 0.1% for BGO, 9.3 ± 0.1% for GSO(Ce) and 12.4 ± 0.1% for YAP(Ce) crystals (see Table 3). As can be seen in Table 2, these scintillators have peak emission at relatively short wavelength (350–480 nm), where the APD is less sensitive (QE ~60% at 390 nm) compared to CsI(Tl) crystal. Nevertheless, QE is still much larger for the APD than that of the PMT (QE ~20%), resulting in better energy resolutions.

### 3.2.1. Number of e–h pairs

Our next concern is to estimate the number of primary e–h pairs produced in the APD for scintillation detection. This can be easily done by making reference to the gain observed with APD in direct X-ray detection and light pulses [8].

Table 4
Number of primary e–h pairs and $E_{th}$ measured with S8664-1010N at 20°C

| Crystal | Shaping time (μs) | Number of primary e–h pairs (pairs/keV) | Minimum detectable energy (keV) |
|---|---|---|---|
| CsI(Tl) | 10 | 28 ±2[a] | 10.2 |
| BGO | 3 | 4.2 ±0.3[b] | 48.8 |
| GSO(Ce) | 1 | 4.3 ±0.3[b] | 44.5 |
| YAP(Ce) | 0.5 | 2.4 ±0.2[b] | 59.4 |

[a]Gain is corrected with a 525 nm LED.
[b]Gain is corrected with a 468 nm LED.

We measured number of primary e–h pairs of four scintillators by illuminating 662 keV γ-rays from a $^{137}$Cs source, comparing with 5.9 keV X-rays from a $^{55}$Fe source as a reference. To consider gain difference between X-rays and scintillation photons, we corrected their pulse heights using the gain ratio of 5.9 keV X-rays to 468 nm or 525 nm of LED photons (see Section 2). Calculated number of primary e–h pairs were 28 ± 2 pairs/keV for CsI(Tl), 4.2 ± 0.3 pairs/keV for BGO, 4.3 ± 0.3 pairs/keV for GSO(Ce) and 2.4 ± 0.2 pairs/keV for YAP(Ce), (see Table 4).

### 3.2.2. Minimum detectable energy

Since reverse-type APDs have low leakage current, they are less affected by noise contribution. To quantify its minimum detectable energy (energy threshold), we removed γ-ray sources and measured the noise spectra. Minimum detectable energy ($E_{th}$) was defined as an energy where the noise count reaches a certain flux level (1 count/s for our case). Table 4 shows $E_{th}$ for different scintillators, measured at 20°C where the energy resolutions were optimum. The CsI(Tl) crystal was achieved at the lowest energy threshold of 10.2 keV for the APD, which is twice larger than that for S8664-55 [5]. This is because S8664-1010N (10 × 10 mm$^2$) has larger capacitance and leakage current than S8664-55, resulting in larger noise contribution.

The minimum detectable energy measured with BGO, GSO(Ce), YAP(Ce) crystals were 48.8, 44.5 and 59.4 keV, respectively. Generally speaking, minimum detectable energy is determined by the balance between the dark noise contribution and the gain amplification. While increasing the bias voltage, APD gain increases and the signal-to-noise ratio should improve. However, the dark noise and excess noise factor also increases. Therefore, the bias voltage which realizes the best energy resolution and that realizes lowest $E_{th}$ may not coincide with each other. For CsI(Tl) crystals the minimum detectable energy was almost unchanged if enough high voltage was applied ($\geqslant$300 V). In contrast the minimum detectable energy improves with increasing the bias voltage for other scintillators. For example, $E_{th}$ was 59.4 keV at 380 V, but improved to be 20 keV at 415 V for YAP(Ce) crystal.

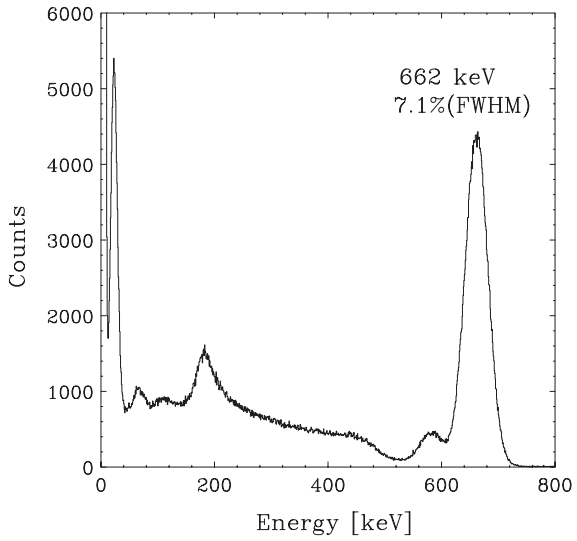


Fig. 10. The energy spectrum of $^{137}$Cs measured with S8664-1010N coupled to a BGO crystal at −20°C.

### 3.3. Performance at low temperature

Next we study the performance of the APD at lower temperature (−20°C). When the APD is cooled down, the dark current decreases significantly and hence expected to improve the signal-to-noise ratio. This effect is remarkable for BGO and GSO(Ce) scintillators whose light output increases with decreasing temperature. Fig. 10 shows the energy spectrum of $^{137}$Cs at −20°C obtained with the APD coupled to a BGO crystal. We achieved the energy resolution of $7.1 \pm 0.2\%$ for 662 keV γ-rays. Comparing with Fig. 7, noise level decreased significantly and 32 keV X-ray peak is clearly detected. The minimum detectable energy was 11.3 keV. Primary e–h pairs was about $6.1 \pm 0.4$ pairs/keV, which is about 1.5 times larger than that obtained at 20°C.

Table 5 lists the energy resolution (for 662 keV), number of e–h pairs, and minimum detectable energy of four different crystals measured at −20°C. Both the energy resolution and the minimum detectable energy improve significantly, except for the CsI(Tl) crystal, where the minimum detectable energy decreased to 3.1 keV but the energy resolution becomes a little bit worse ($5.9 \pm 0.1\%$). For the CsI(Tl) crystal, light output from scintillators is known to decrease about 10% compared to that of 20°C, which may affect the energy resolution. The energy resolutions measured with the GSO(Ce) and the YAP(Ce) crystals were $7.1 \pm 0.2\%$ and $10.7 \pm 0.2\%$, respectively. The minimum detectable energy also improves significantly to 14.3 keV (GSO(Ce)) and 43.6 keV (YAP(Ce)).

#### 3.3.1. Readout of large scintillators

Large-area APDs can effectively collect weak scintillation light from large size crystals. As an application, we tried to read out a large BGO crystal ($300 \times 48\,mm^2$ plate of 3 mm thickness) with the $10 \times 10\,mm^2$ APD (S8664-1010N). The schematic view of the sensor is shown in Fig. 11. Signals from the BGO crystal were transmitted to the APD through a light-guide. Fig. 12 presents an energy spectrum of $^{137}$Cs measured at −15°C. Despite significant mismatch of the scintillator size and the APD surface area, this APD was able to collect a large number of scintillation photons. A good energy resolution of $20.9 \pm 0.2\%$ was obtained for 662 keV γ-rays with the minimum detectable energy of about 60 keV.

This result suggests various possibilities of using APDs for future applications. For example, we have a plan to use APDs for Japan's future X-ray

Table 5
Energy resolutions, e–h pairs, and $E_{th}$ measured with S8664-1010N at −20°C

| Crystal | Shaping time (μs) | Energy resolution of 662 keV (%) | Number of primary e–h pairs (pairs/keV) | Minimum detectable energy (keV) |
|---|---|---|---|---|
| CsI(Tl) | 10 | 5.9 ± 0.1 | 25 ± 2[a] | 3.1 |
| BGO | 3 | 7.1 ± 0.2 | 6.1 ± 0.4[b] | 11.3 |
| GSO(Ce) | 2 | 7.1 ± 0.2 | 6.0 ± 0.4[b] | 14.3 |
| YAP(Ce) | 0.5 | 10.7 ± 0.2 | 2.8 ± 0.2[b] | 43.6 |

[a]Gain is corrected with a 525 nm LED.
[b]Gain is corrected with a 468 nm LED.

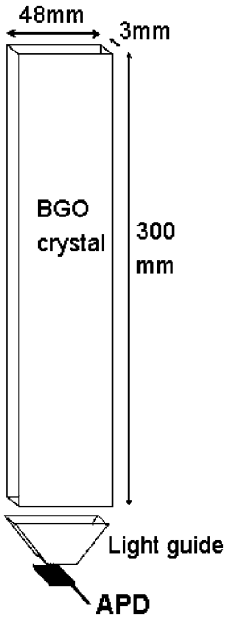


Fig. 11. A schematic view of BGO plate coupled to S8664-1010N.

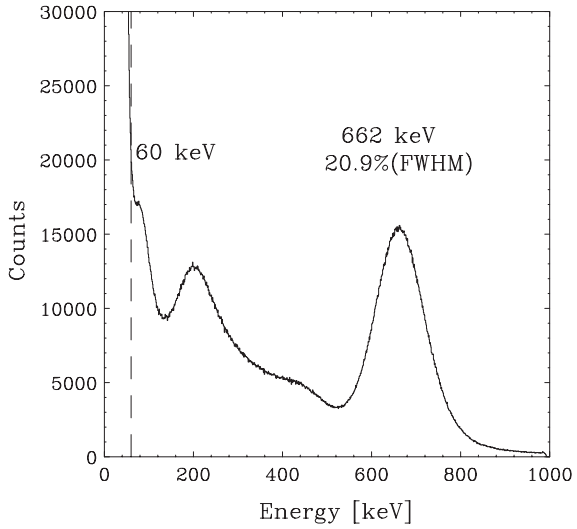


Fig. 12. The energy spectrum of $^{137}$Cs measured with S8664-1010N coupled to a large BGO plate at −15°C.

astronomy mission *NeXT*, which is planned to be launched in ~2011 [7]. The *NeXT* mission is a successor to the *ASTRO-E2* mission (planned to be launched in 2005), with much higher sensitivity in the energy from 0.5 keV to 1 MeV. In the energy range above 100 keV, shielding against background becomes important because signals from celestial sources are much weaker than the background events, some from diffuse cosmic γ-rays and others may have atmospheric origin. Moreover, geomagnetically trapped particles and primary cosmic rays are also a big matter. The phoswich configuration and a tight and active "well-type" shield is a good solution to reduce the background significantly.

In the case of Hard X-ray Detector (HXD) on board *ASTR0-E2* satellite, the well-type shield made of BGO scintillators are surrounding the detection part (GSO scintillators and PIN diode) to reduce the background (Fig. 13) [9]. In this case, single PMT will read out scintillation light from the detection part (GSO), bottom BGO (bottom part of the phoswich counter), and Well BGO (collimator part of the phoswich counter) altogether. Obviously, the light yields from the Well BGO must be smaller than that of the Bottom BGO due to loss or attenuation of scintillation light before reaching the PMT cathode (by a factor of 2). This configuration inevitably raises the

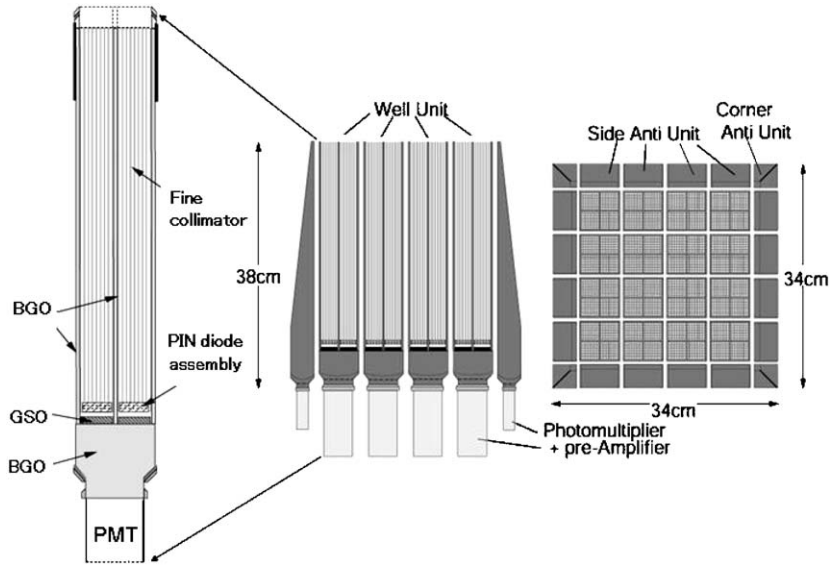


Fig. 13. The configuration of the Hard X-ray Detector (HXD) assembly onboard *ASTRO-E*2 satellite: (left) closeup of one unit, (center) side-view, (right) top-view.

minimum detectable energy of Well BGO and thus lower the sensitivity to the background rejection. For example, 100 keV γ-rays hitting Well BGO is difficult to reject for the HXD configuration.

In order to further reduce the background and thus to improve the sensitivity, we have proposed a new detector called the Soft Gamma-ray detector (SGD) for the *NeXT* mission, which utilizes the idea of a narrow FOV Compton telescope as shown in Fig. 14 [7]. In the SGD, we combine a stack of Si strip detectors and CdTe pixel detectors as a detection part, which is mounted inside the well-type BGO active shield. We are planning to use APDs to read out Well and Bottom BGO scintillators, instead of PMTs. Dimensions of Well BGO plate will be similar to that tested in this paper (Fig. 11).

Since the APD is very compact and have rugged structure, we can directly couple APD with BGO plate to read out weak scintillation photons. Such configuration should improve the sensitivity to the low-energy γ-ray and particle background rejection, without significant loss of scintillation light. We have shown that the minimum detectable energy is as low as 60 keV for the APD plus BGO plate system, but we expect that $E_{\mathrm{th}}$ can be further improved since (1) APD size is still far from optimum and (2) significant fraction of scintillation light may be lost when transmitting the light guide. We will develop new types of large-area APDs (e.g., $50 \times 3\,\mathrm{mm}^2$ surface area) which can directly couple to Well BGO plate, and hope to improve the minimum detectable energy as low as 30 keV.

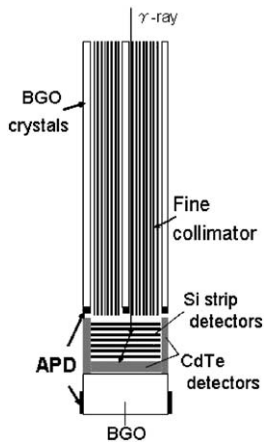


Fig. 14. The configuration of a unit of SGD onboard the *NeXT* satellite.

## 4. Conclusion

We have studied the performance of a large area ($10 \times 10\,mm^2$), reverse-type APD developed by Hamamatsu photonics. We showed that leakage current is as low as 2–3 nA at room temperature and the gain stabilities are 3.3%/V and $-2.5\%/^{\circ}C$. We showed the performance as a $\gamma$-ray detectors with different scintillators, CsI(Tl), BGO, GSO(Ce), and YAP(Ce). A good energy resolution of $4.9 \pm 0.2\%$ (FWHM) was obtained for 662 keV $\gamma$-rays from a $^{137}Cs$ source as measured with a CsI(Tl) crystal. The minimum detectable energy was as low as 10.2 keV at $20^{\circ}C$ and 3.1 keV at $-20^{\circ}C$. The energy resolutions for 662 keV $\gamma$-rays were $8.3 \pm 0.3\%$ for BGO, $7.8 \pm 0.2\%$ for GSO(Ce), $11.3 \pm 0.3\%$ for YAP(Ce) at $20^{\circ}C$. When the APD is cooled down, the energy resolutions of BGO, GSO(Ce) and YAP(Ce) crystals were improved to be $7.1 \pm 0.2\%$, $7.1 \pm 0.2\%$, $10.7 \pm 0.2\%$, respectively, at $-20^{\circ}C$.

Thanks to its high quantum efficiency and low noise contribution, we showed that the APD is also suitable to read out scintillation light from large scintillators. As the first step for the future X-ray astronomy mission *NeXT*, we tested a BGO plate ($300 \times 48\,mm^2$ of 3 mm thickness) coupled with the APD. We obtained a good energy resolution of $20.9 \pm 0.2\%$ for 662 keV $\gamma$-rays and achieved the minimum detectable energy of 60 keV. Our studies confirm that large area APD may be superior to the traditional PMTs in some applications, such as compact scintillation light sensor used in space near future.

## References

[1] J.P. Pansart, Nucl. Instr. and Meth. A 387 (1997) 186.
[2] M. Moszyński, M. Kapusta, M. Balcerzyk, M. Szawlowski, D. Wolski, I. Wegrecka, M. Wegrzecki, IEEE Trans. Nucl. Sci. NS-48 (2001) 1205.
[3] K. Deiters, et al., Nucl. Instr. and Meth. A 442 (2000) 193.
[4] R. Lecomte, C. Pepin, D. Rouleau, H. Dautet, R.J. McIntyre, D. McSween, P. Webb, Nucl. Instr. and Meth. A 423 (1999) 92.
[5] T. Ikagawa, et al., Nucl. Instr. and Meth. A 515 (2003) 671.
[6] P.P. Webb, R.J. McIntyre, J. Cornadi, RCA Rev. 35 (1974) 234.
[7] T. Takahashi, et al., New Astron. Rev. 48 (2004) 269.
[8] M. Moszyński, M. Szawlowski, M. Kapusta, M. Balcerzyk, Nucl. Instr. and Meth. A 485 (2002) 504.
[9] M. Tashiro, et al., IEEE Trans. Nucl. Sci. NS-49 (2002) 1893.
[10] J. Kataoka, et al., SPIE. 5501 (2004) 249.
[11] J. Grahl, et al., Nucl. Instr. and Meth. A 504 (2003) 44.
[12] R.J. McIntyre, P.P. Web, H. Dautet, IEEE Trans. Nucl. Sci. NS-43 (1996) 1341.